Supporting Information

Heterostructure SnS/TiO_2@C hollow nanospheres for superior lithium and sodium storage

Yan Zhang,[†a] Hang Su,[†a] Canpei Wang,[a] Dingcheng Yang,[a] Yongsheng Li,[a] Wenbo Zhang,[a] Hongqiang Wang,[b] Jianmin Zhang,*[a] Dan Li,*[a]

a College of Chemistry and Molecular Engineering, Zhengzhou University, Zhengzhou, 450001, P. R. China

b College of Chemistry & Environment Science, Hebei University, Baoding, 071002, P. R. China

* Corresponding authors.

E-mail addresses: danli@zzu.edu.cn (D. Li), zhjm@zzu.edu.cn (J. Zhang)

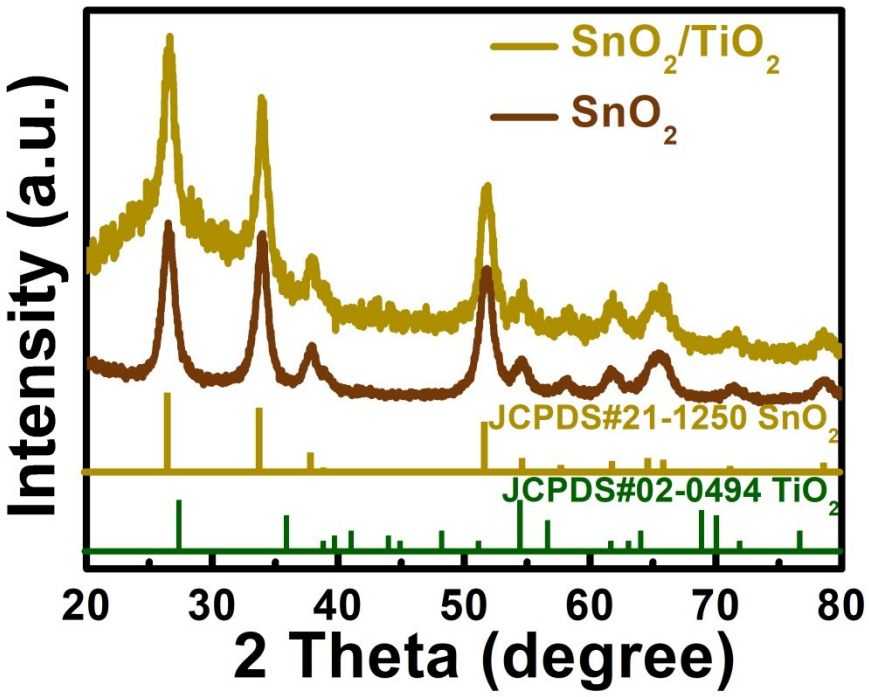

Fig. S1 XRD patterns of as-prepared SnO_2 and SnO_2/TiO_2.

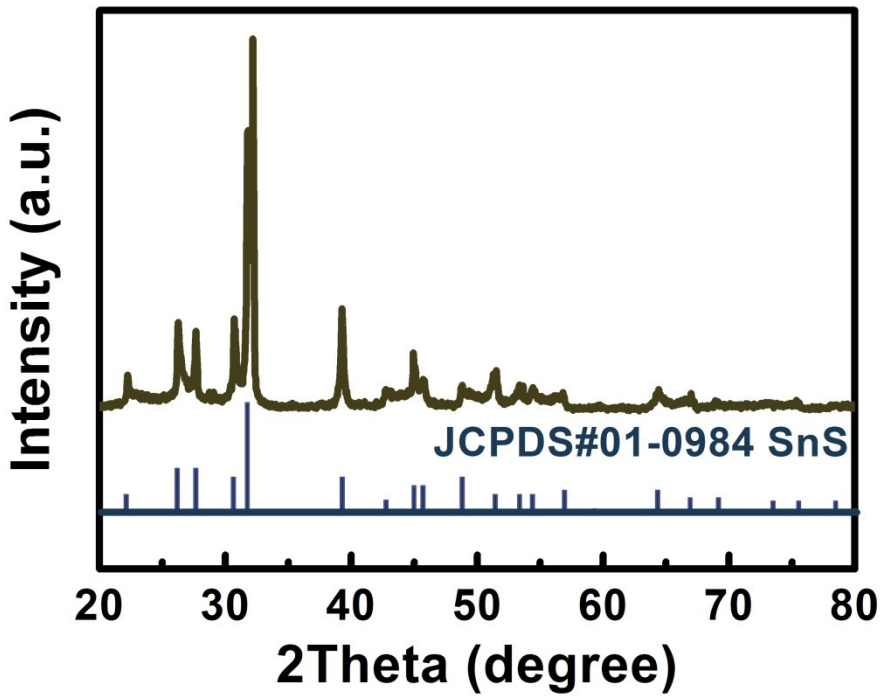

Fig. S2 XRD pattern of as-prepared SnS@C hollow nanospheres.

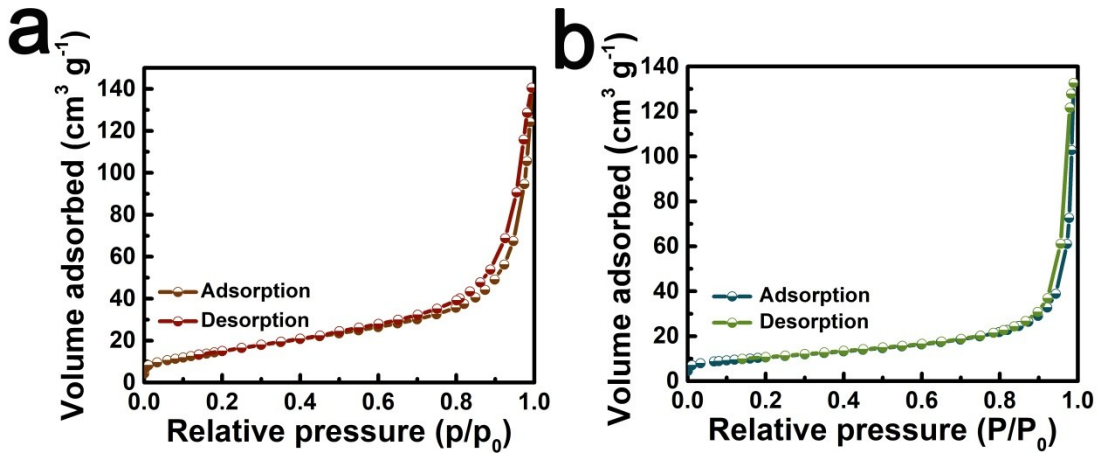

Fig. S3 N_2 adsorption-desorption isotherms of (a) SnS/TiO_2@C and (b) SnS@C.

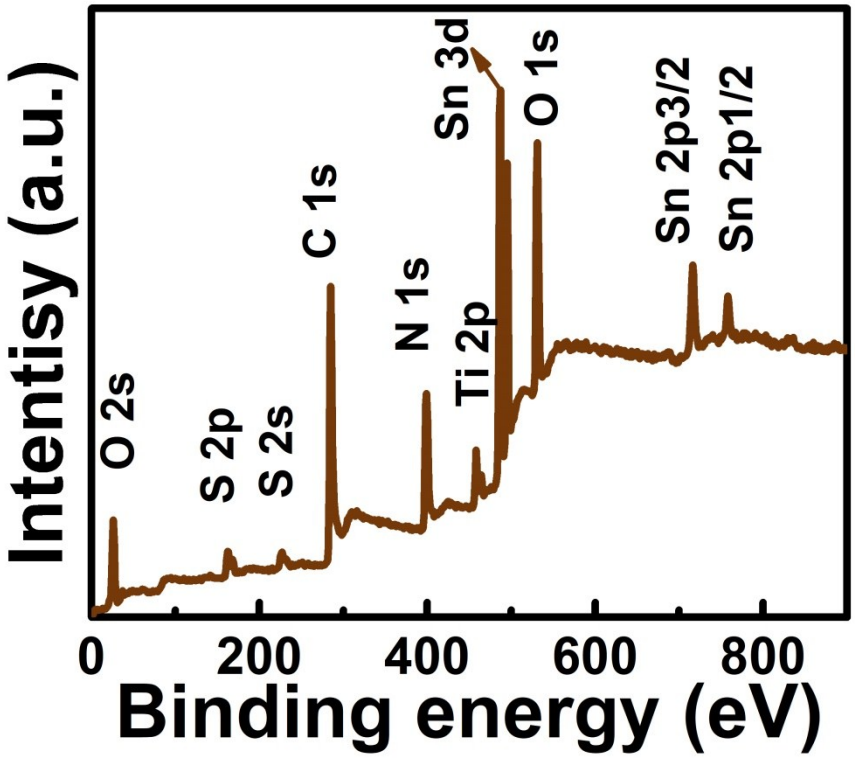

Fig. S4 Survey XPS spectrum of SnS/TiO_2@C.

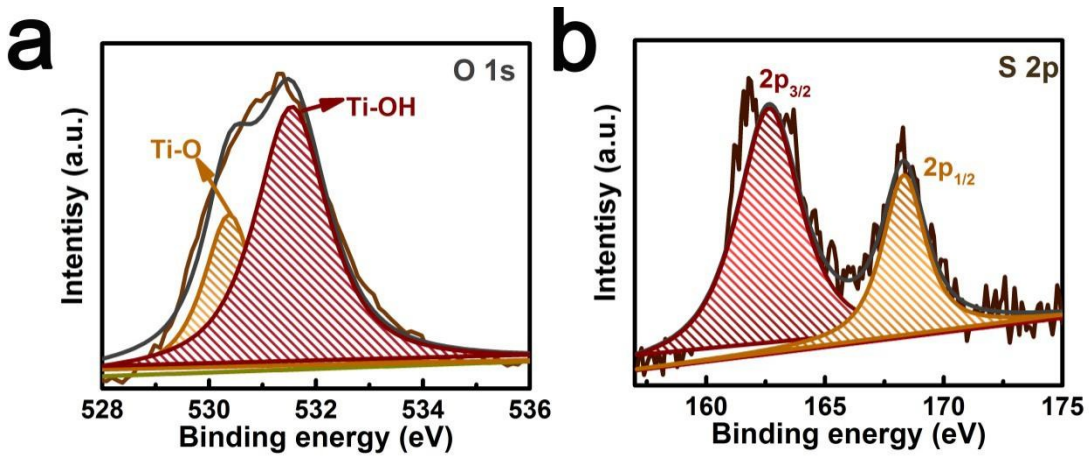

Fig. S5 XPS spectra of (a) O 1s and (b) S 2p in SnS/TiO_2@C.

The spectrum of O 1s can be deconvoluted into two peaks at 530.4 and 531.6 eV, owing to Ti-O and Ti-OH bonds of TiO_2. [1] The S 2p peak can be fitted into two peaks at 162.7 and 167.4 eV, corresponding to S^{2-}. [2]

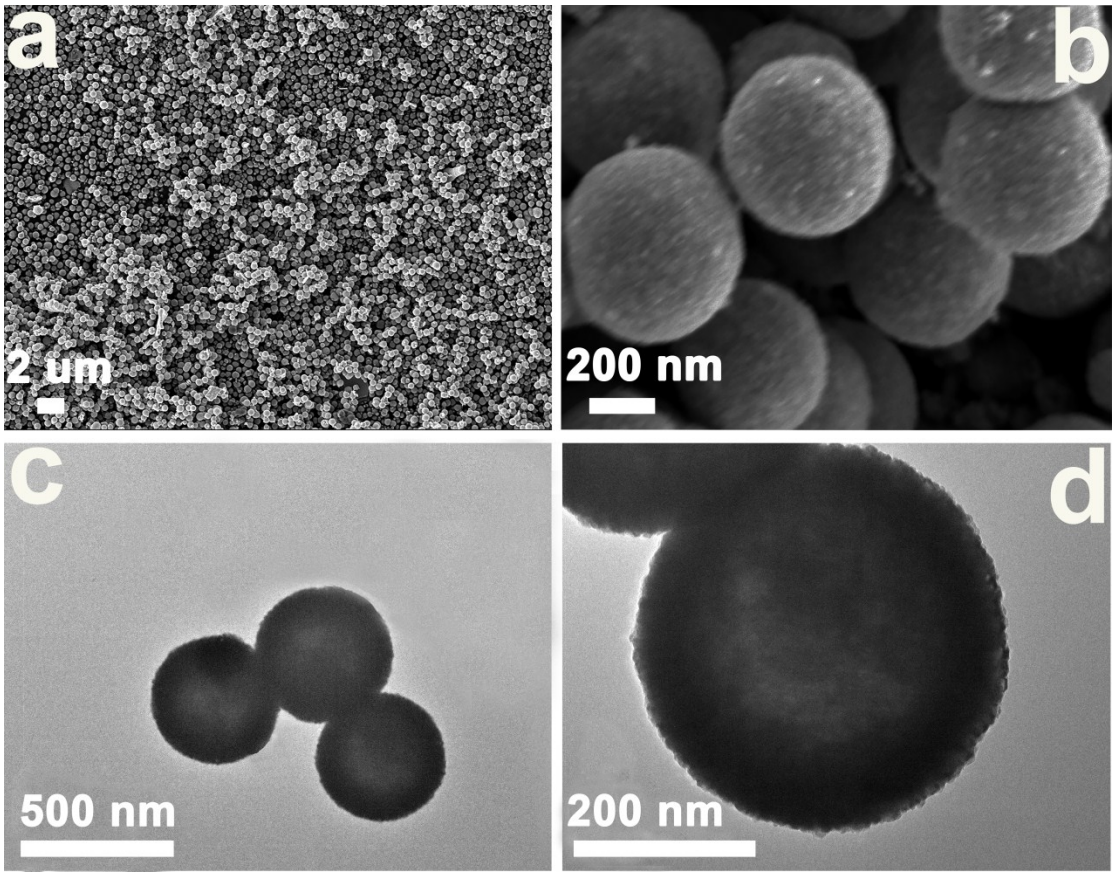

Fig. S6 (a, b) SEM and (c, d) TEM images of the SnO_2 hollow nanospheres.

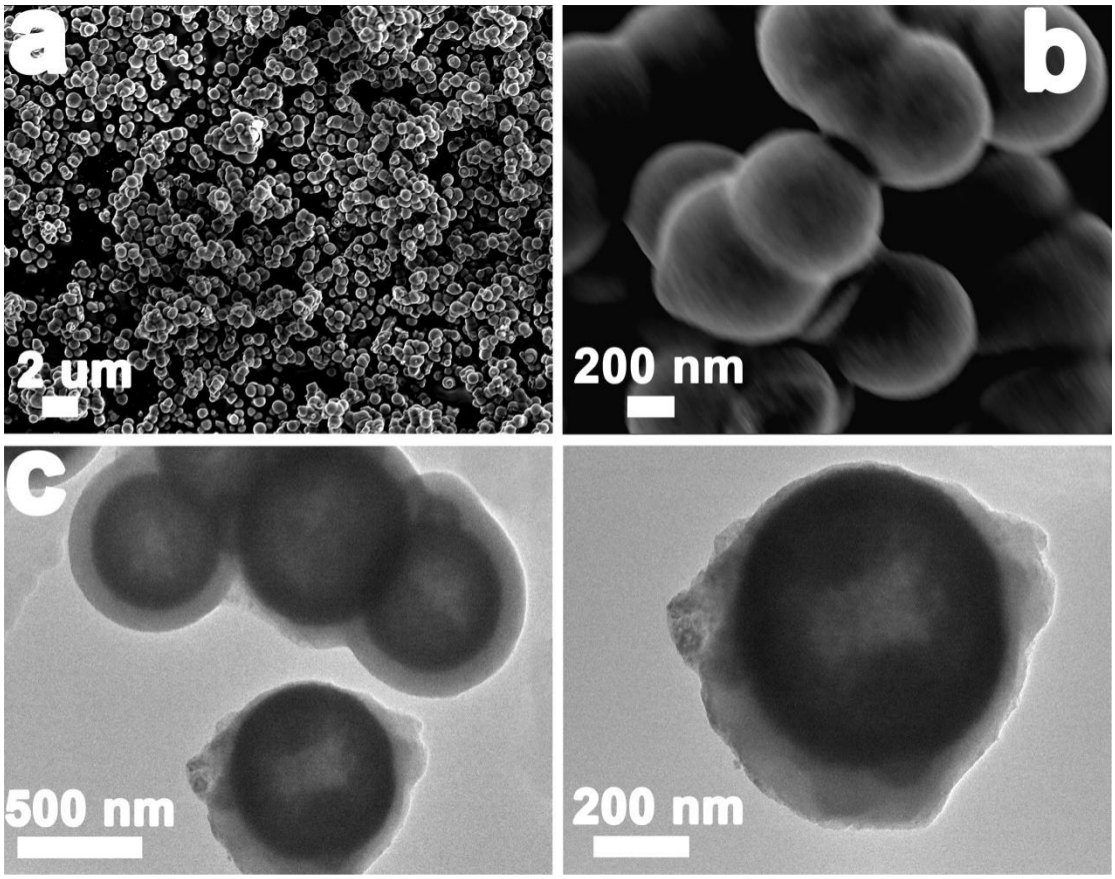

Fig. S7 (a, b) SEM and (c, d) TEM images of the SnO_2/TiO_2 intermediate.

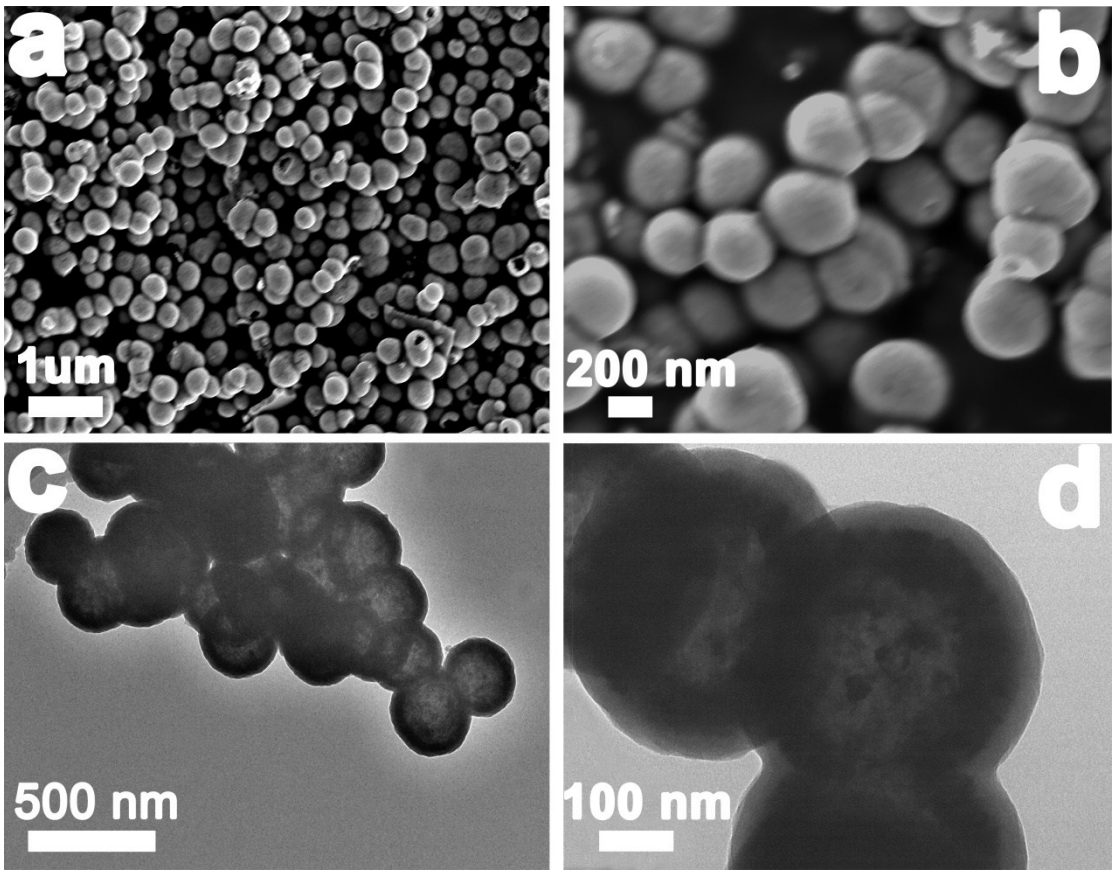

Fig. S8 (a, b) SEM and (c, d) TEM images of SnS@C.

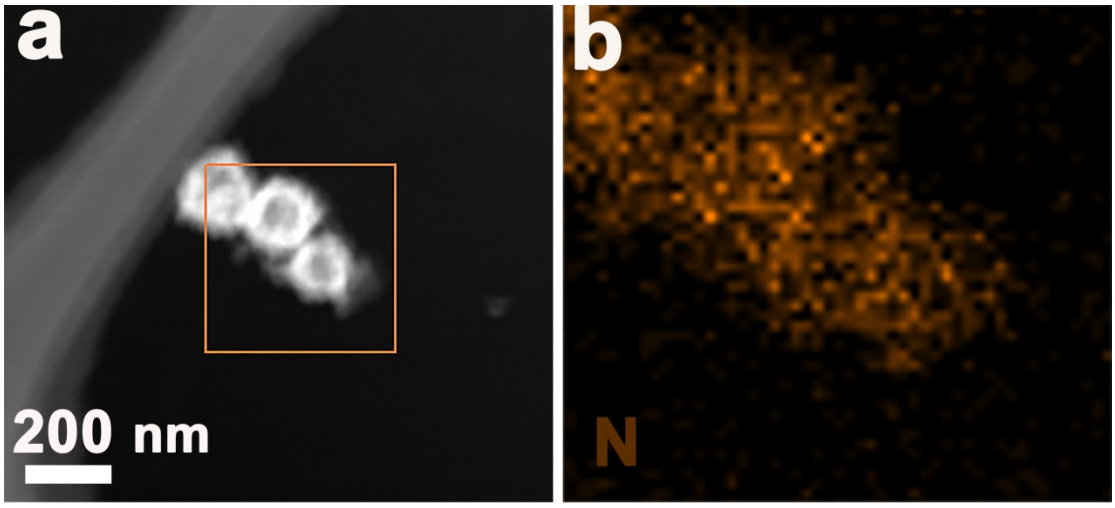

Fig. S9 (a) TEM image of SnS/TiO_2@C, (b) elemental mapping image of N in SnS/TiO_2@C.

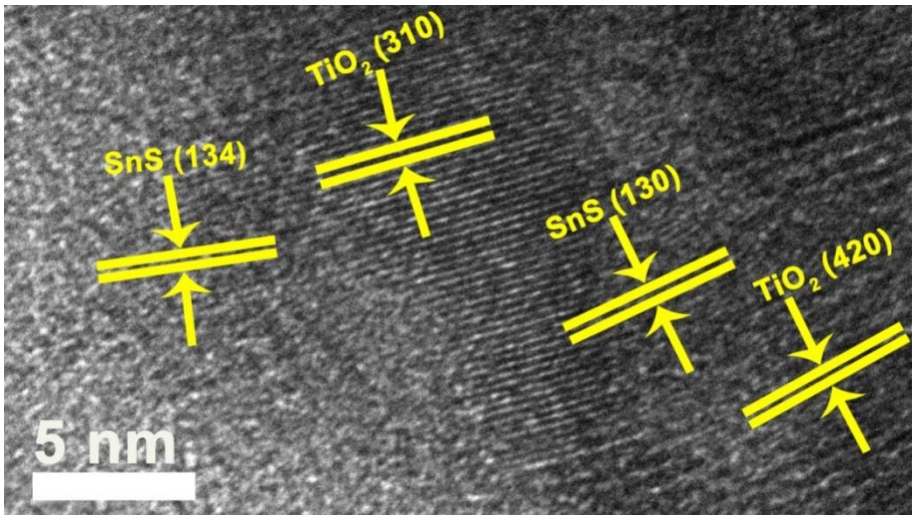

Fig. S10 HRTEM images of SnS/TiO_2@C.

The marked lattices with *d*-spacing were measured to be 0.122 and 0.134 nm, which are consistent well with the (134) and (130) plans of orthorhombic SnS, respectively. While the *d*-spacing of 0.143 and 0.098 nm assign to the (310) and (420) planes of tetragonal TiO_2, demonstrating the formation of hetero-interface, which can improve electrochemical reaction kinetics and the movement of ions and electrons.

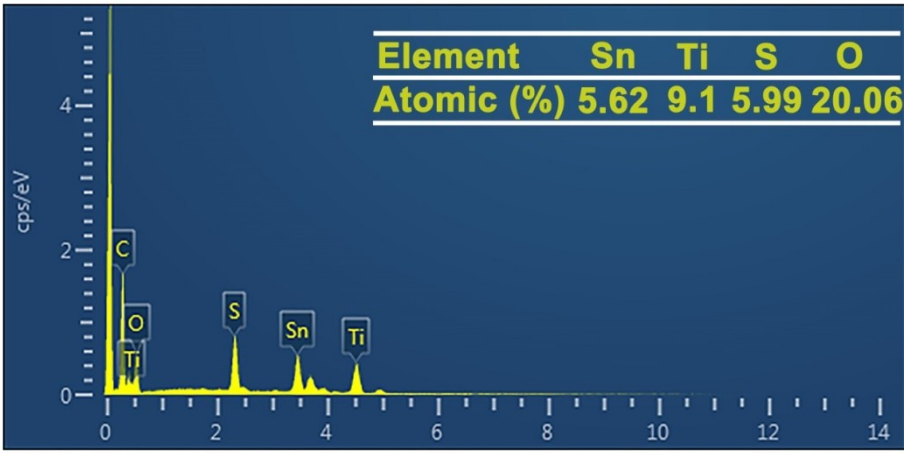

Fig. S11 EDS spectrum of SnS/TiO_2@C.

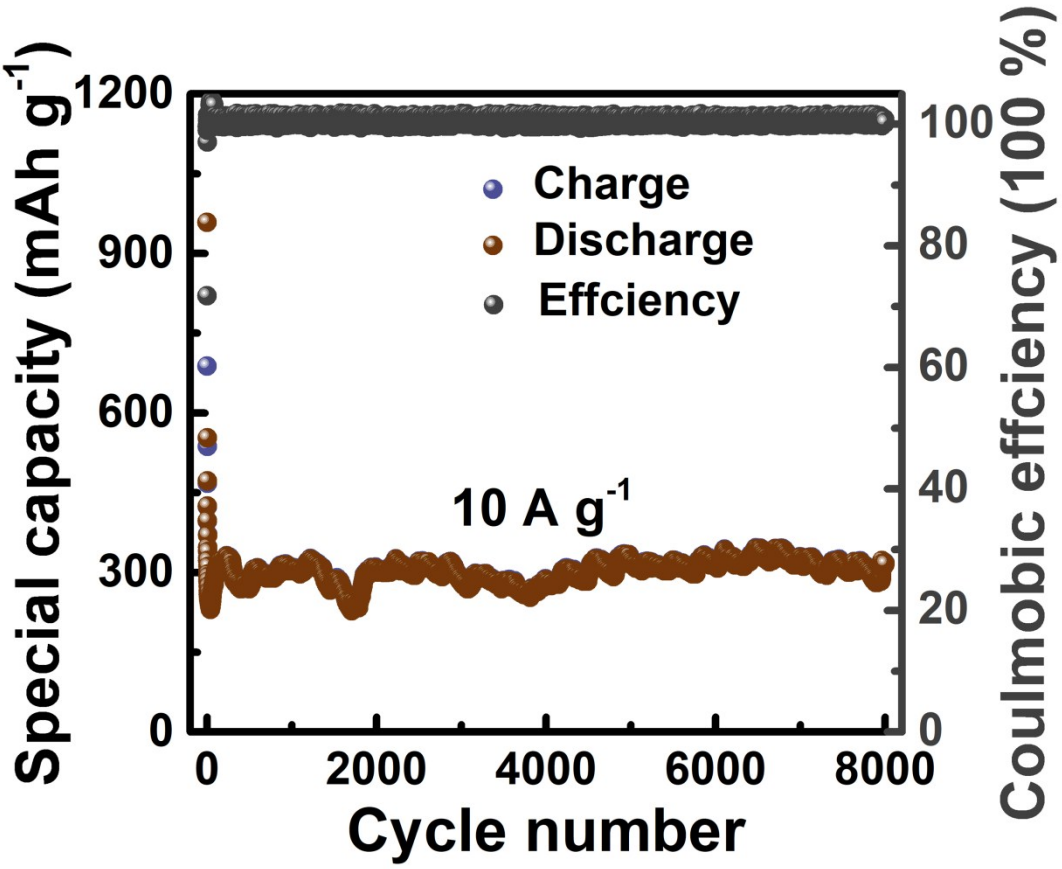

Fig. S12 Long-term cycling performance of SnS/TiO_2@C at a current density of 10 A g^{-1} for LIBs.

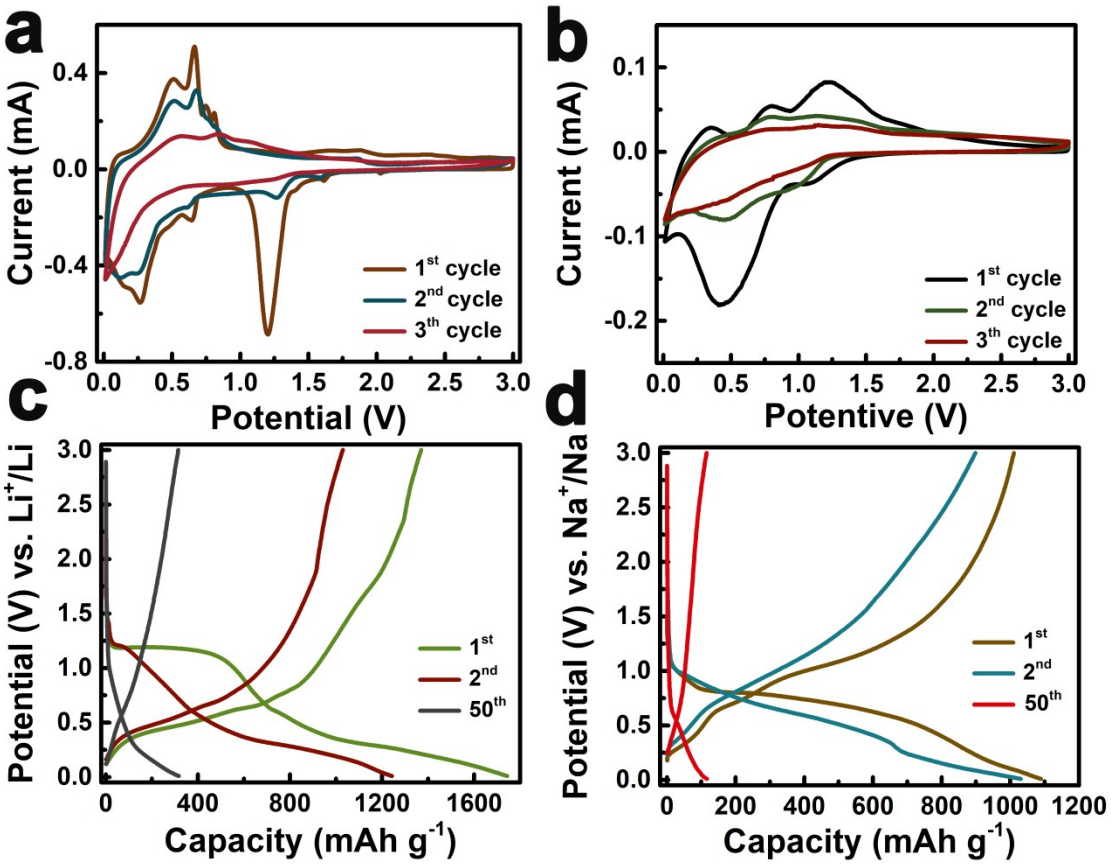

Fig. S13 CV curves of SnS@C at a scan rate of 0.1 mV s^{-1} for the first cycles for (a) LIBs and (b) SIBs, and the galvanostatic charge/discharge profiles at different cycles (c) at a current density of 0.5 A g^{-1} for LIBs and (d) at a current density of 0.2 A g^{-1} for SIBs.

Fig. S13a shows the cyclic voltammograms (CV) curves of the first three cycles of SnS@C electrode in the potential range of 0.01–3 V versus Li^+/Li at a scan rate of 0.1 mV s^{-1}. During the first discharge process, a sharp peak located at 1.23 V can be observed, corresponding to the conversion reaction of SnS and the irreversible formation of solid-electrolyte interphase (SEI) layer. Besides, cathodic peaks located at 0.65 V and 0.26 V is related to the multistep alloying reaction. In the charging process, the multiple anodic peaks in the range of 0.5-0.68 V are associated with the multistep dealloying process. Moreover, the peak located at 1.89 V is assigned to the conversion of Sn to SnS. For the electrochemical properties of SnS@C for SIBs, the

CV curves of the first three cycles was characterized and shown in Fig. S13b. In the first cathodic scan, a peak at 1.1 V corresponds to the conversion reaction of SnS to Sn and Na_2S. The peak nears to 0.5 V is ascribed to the formation of Na-Sn alloys and SEI layer. In the first anodic scans, the peaks at 0.33 V and 0.79 V can be attributed to the multistep dealloying processes of Na_xSn to Sn metal. The oxidation peaks at 1.23 V suggests that the conversion from Sn to SnS is reversible. In sequence cycles, the reduction peak at 0.5 V shifts to 0.55 V, which is corresponded to the alloying reaction of Sn.

Fig. S13c displays the discharge/charge profiles of SnS@C at the 1st, 2nd, and 50th cycles under a current density of 0.5 A g^{-1} for LIBs. Clearly, the first discharge plateau around 1.23 V is attributed to the conversion of SnS to Sn and Li_2S, as well as the formation of SEI layer. The sloping plateau from 0.6 to 0.2 V corresponds to the alloying reaction of Sn. The charge plateau presents from 0.5 to 0.68 V, indicating the dealloying reaction. While, the charge plateau at 1.91 V is assigned to the reversible formation of SnS. Fig. S13d shows the 1st, 2nd, and 50th charge/discharge profiles of the SnS@C electrode at a current density of 0.2 A g^{-1} for SIBs. The first discharge process presents a plateau around 1.0 V, which corresponds to the decomposition of SnS. The second plateau exhibits a sloping plateau from 0.6 to 0.5 V, corresponding to the formation of Na_xSn and SEI layer. Similarly, the charge curve presents two sloping plateaus at 0.4 and 0.75 V, suggesting the multistep dealloying reaction. The third sloping charge plateau at 1.25 V corresponds to the formation of SnS. These results are consistent with the CV results.

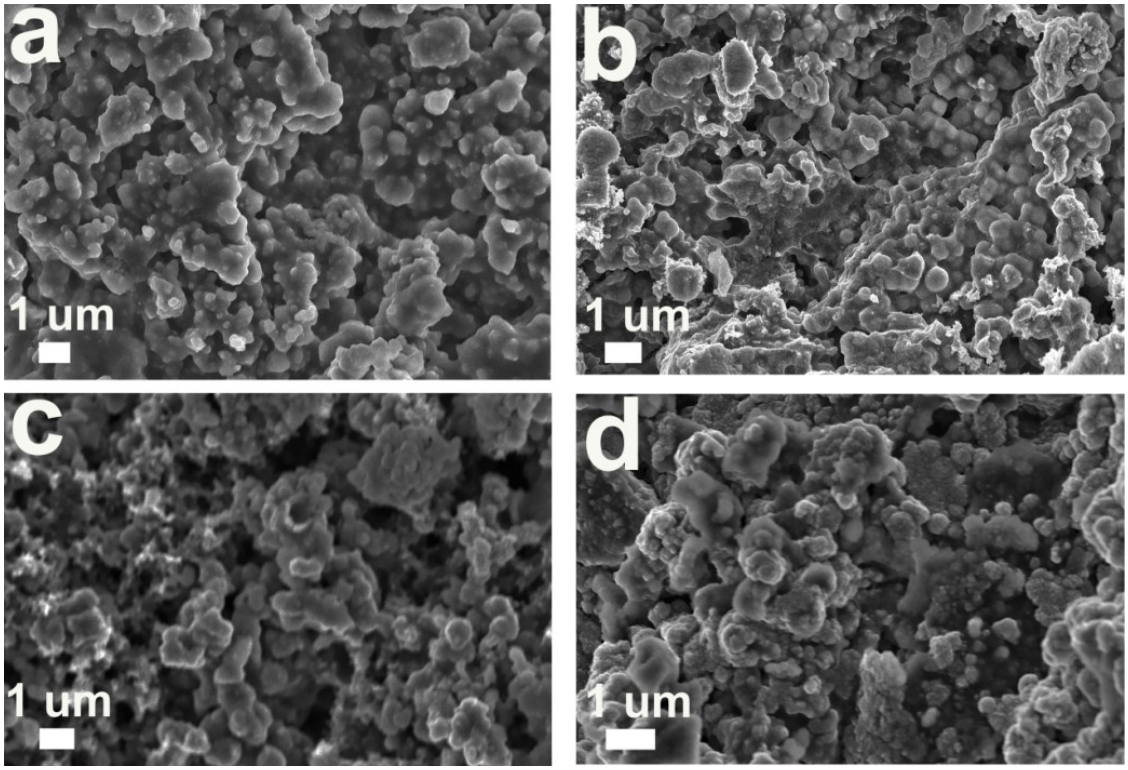

Fig. S14 SEM images of (a) SnS/TiO_2@C and (b) SnS@C after 3000 cycles for LIBs, (c) SnS/TiO_2@C and (d) SnS@C after 700 cycles for SIBs at a current density of 5 A g^{-1}.

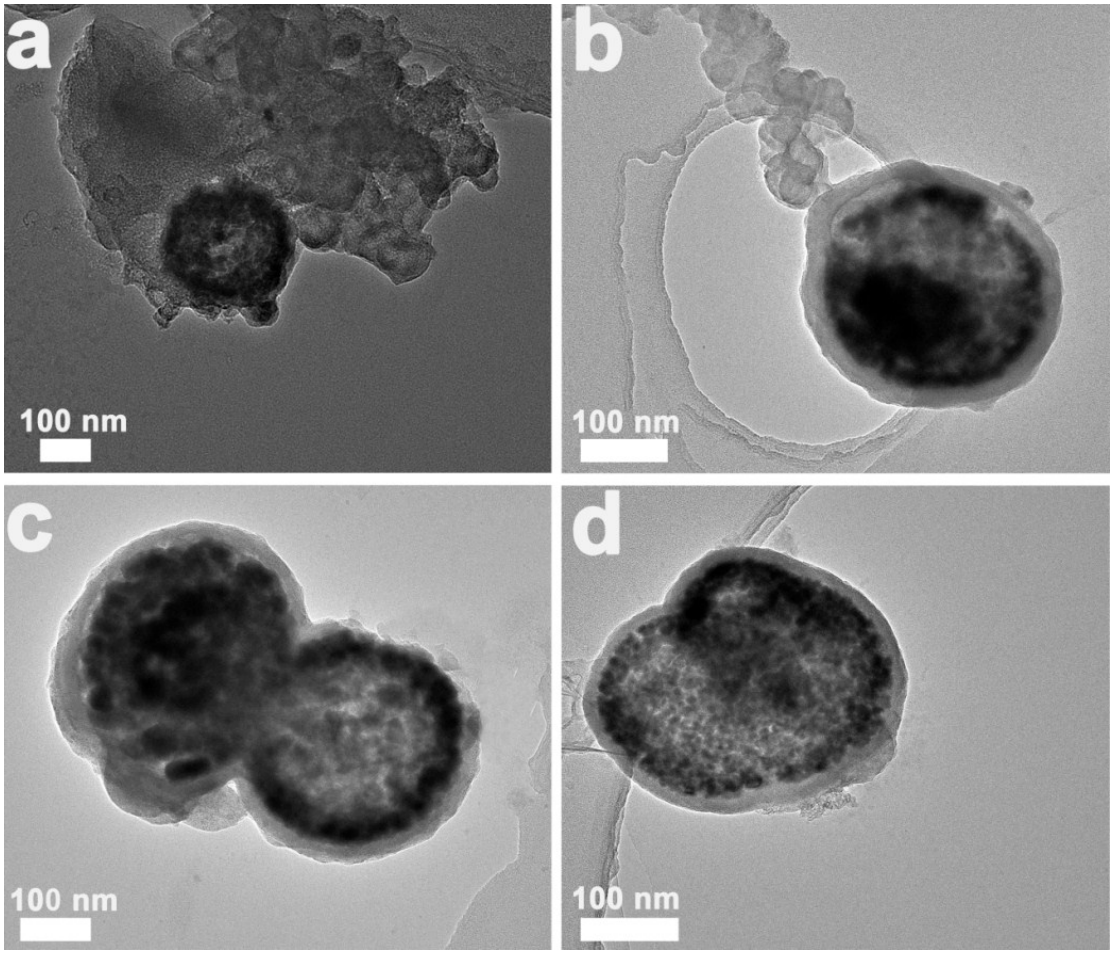

Fig. S15 TEM images of (a) SnS/TiO_2@C and (b) SnS@C after 3000 cycles for LIBs, (c) SnS/TiO_2@C and (d) SnS@C after 700 cycles for SIBs at a current density of 5 A g^{-1}.

As shown in Fig. S14 and Fig. S15, the structure of SnS/TiO_2@C and SnS@C well maintained after long-term cycling for LIBs and SIBs. Notably, the spherical structure became more porous and the diameter has increased to some extent, which can be ascribed to the insertion and extraction of the ions during the electrochemical reactions.

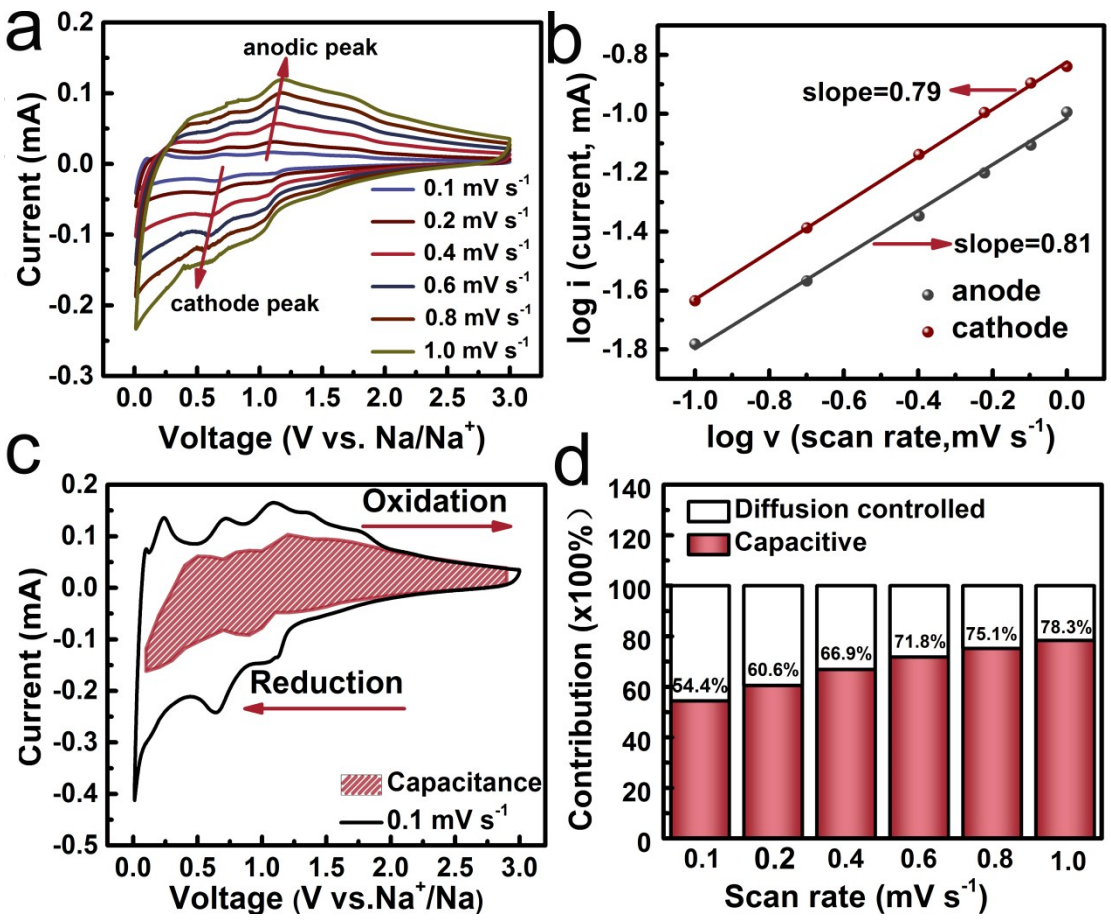

Fig. S16 Quantitative capacitive research of sodium storage behavior of SnS/TiO_2@C: (a) CV curves at different scan rates, (b) relationship between log *i* and log *v*, (c) capacitive contribution to the charge storage at 0.1 mV s^{-1}, (d) contributions of diffusion-controlled and capacitance-controlled to the total capacity at different scan rates.

In order to explore the reasons for the excellent cycling and rate performance of SnS/TiO_2@C, the kinetic analysis of the sodium ion energy storage was conducted. The CV curves of the SnS/TiO_2@C electrode at scan rates ranging from 0.1 to 1 mV s^{-1} were shown in Fig. S16a. Moreover, the proportion of the surface capacitance can be characterized by the relationship based on the following equation:

$$i=av^b \qquad (1)$$

In which *a* and *b* are constants parameters. [3, 4] The *b*-value closed to 0.5 indicates a diffusion-controlled process, whereas close to 1.0 represents a capacitance-controlled

process. Based on the slope of log *i vs.* log *v*, the *b* values of the cathodic and anodic peaks are calculated to be 0.79 and 0.81 (Fig. S16b), respectively. Furthermore, the specific contribution of the capacitance and diffusion to the total storage by can be separated based on the following equation:

$$i = k_1 v + k v^{0.5} \quad (2)$$

In which $k_1 v$ represents the ionic diffusion contribution and $k v^{0.5}$ represent surface capacitance contribution.[5] The pink shadow area in Fig. S16c means the contribution of the surface capacitance at 0.1 mV s^{-1} with a value of about 54.4%. Fig. S16d indicates the contributions of surface capacitance of the SnS/TiO_2@C electrode are 60.6%, 66.9%, 71.8%, 75.1%, and 78.3% at scan rates of 0.2, 0.4, 0.6, 0.8, and 1 mV s^{-1}, respectively.

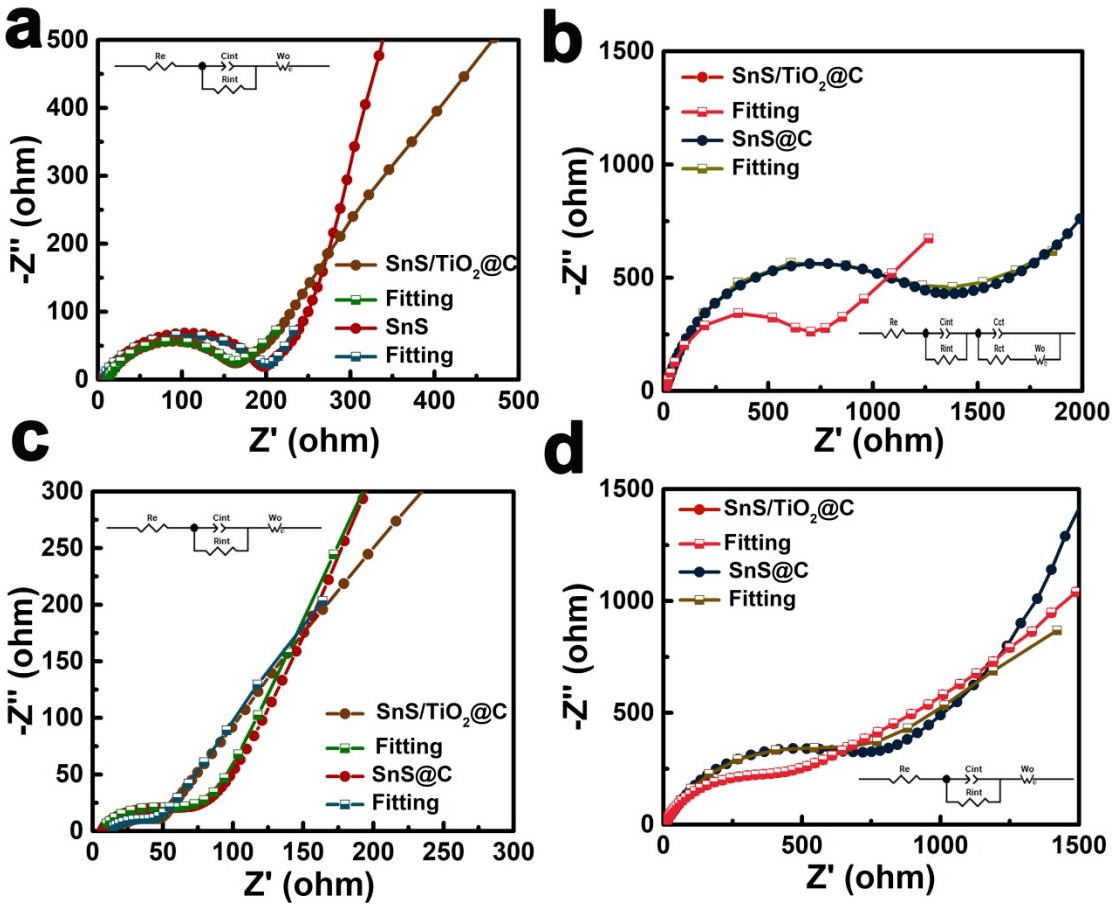

Fig. S17 Nyquist plots of the electrochemical impedance spectra of SnS/TiO_2@C and SnS@C electrodes after 1 cycle for (a) LIBs and (b) SIBs, as well as after 50 cycles at 0.5 A g^{-1} for (c) LIBs and (d) SIBs.

The electrochemical impedance spectroscopy (EIS) (Fig. S17) of SnS/TiO_2@C and SnS@C electrodes were performed after 1 and 50 cycles at 0.5 A g^{-1} for LIBs and SIBs at the fully charging state. In the Nyquist plot, the high frequency semicircle represents the charge transfer resistance (R_{ct}), while the low frequency slop indicates the ion diffusion resistance. After fitting the impedance parameters (Table S1), it can be seen that the R_{ct} + R_f of the SnS/TiO_2@C electrode are smaller that of SnS@C electrode after either 1 or 50 the cycles, indicating the promoted charge transfer and the enhanced reaction kinetics of SnS/TiO_2@C during cycling.[6]

Table S1. Equivalent circuit parameters of the SnS/TiO_2@C and SnS@C electrodes for LIBs and SIBs.

	Sample	R_s/Ohm	$R_{ct}+R_f$
After 1 cycle for LIBs	SnS/TiO_2@C	9.965	140.6
	SnS@C	3.379	195.3
After 50 cycles for LIBs	SnS/TiO_2@C	10.7	36.1
	SnS@C	9	42.65
After 1 cycle for SIBs	SnS/TiO_2@C	3.142	1194.4
	SnS@C	2.213	1561
After 50 cycles for SIBs	SnS/TiO_2@C	1.914	431
	SnS@C	1.592	533.4

Table S2 Comparison of electrochemical performance of SnS-based anodes for LIB and SIB.

Material	Cycling stability (LIB) Capacity/Current/Cycles mA h g^{-1}/A g^{-1}/n	rate capability (SIB) Capacity/Current mA h g^{-1}/A g^{-1}	Ref.
This work	672.4/0.5/100 405.8/5/3000	228.5/5 285.2/2	This work
SnS@N-rGO	229/0.2/200		7
SnS nanoflowers	580/0.05/30		8
SnS /SnSb@C		159/2	9
SnS@graphene	535/0.05/50		10
SnS/C		77/5	11
SnS/CNT		184/0.8	12
N-SnS/SnO2/C	550/0.1/100		13
Porous SnS nanorods/C	466/0.05/50		14
SnS/SnS_2 nanosheets	500/0.1/50		15
SnS/CNTs		252.4/3.2	16
C/SnS@C		190/5	17
SnS	604.6/0.1/80		18
SnS NS/RGO	560/0.1/100		19
3D SnS nanoflower	520/0.05/50		20
SnS/C	542/NA/40		21
3D SnS/C		220/5	22
SnS/PDDA-Ti_3C_2	646/0.1/100		23
SnS HNF		228/2	24
S-SnS nanospheres		235/3.2	25

References

1. Q. H. Tian, L. X. Y. Li, J. Z. Chen, L. Yang and S. Hirano, *Journal of Power Sources*, 2018, **376**, 1-10.
2. P. V. Prikhodchenko, D. Y. W. Yu, S. K. Batabyal, V. Uvarov, J. Gun, S. Sladkevich, A. A. Mikhaylov, A. G. Medvedev and O. Lev, *J. Mater. Chem. A*, 2014, **2**, 8431-8437.
3. K. Zhang, Z. Hu, X. Liu, Z. L. Tao and J. Chen, *Adv. Mater.*, 2015, **27**, 3305-3309.
4. D. L. Chao, P. Liang, Z. Chen, L. Y. Bai, H. Shen, X. X. Liu, X. H. Xia, Y. L. Zhao, S. V. Savilov, J. Y. Lin and Z. X. Shen, *ACS Nano*, 2016, **10**, 10211-10219.
5. X. J. Wei, C. J. Tang, Q. Y. An, M. Y. Yan, X. P. Wang, P. Hu, X. Y. Cai and L. Q. Mai, *Nano Res.*, 2017, **10**, 3202-3211
6. X. C. Li, G. L. Guo, N. Qin, Z. Deng, Z. G. Lu, D. Shen, X. Zhao, Y. Li, B. L. Su and H. E. Wang, *Nanoscale*, 2018, **10**, 15505-15512.
7. D. H. Youn, S. K. Stauffer, P. H. Xiao, H. Park, Y. J. Nam, A. Dolocan, G. Henkelman, A. Heller and C. B. Mullins, *ACS Nano*, 2016, **10**, 10778-10788.
8. D. D. Vaughn, O. D. Hentz, S. R. Chen, D. H. Wang and R. E. Schaak, *Chem. Commun.*, 2012, **48**, 5608-5610.
9. J. Zhu, C. Q. Shang, Z. Y. Wang, J. J. Zhang, Y. Liu, S. Gu, L. J. Zhou, H. Cheng, Y. Y. Gu and Z. G. Lu, *ChemElectroChem*, 2018, **5**, 1098-1104.
10. H. C. Tao, X. L. Yang, L. L. Zhang and S. B. Ni, *J. Electroanal. Chem.*, 2014, **728**, 134-139.
11. Y. L. Zhou, Q. Wang, X. T. Zhu and F. Y. Jiang, *Nanomaterials*, 2018, **8**, 9.

12. Y. Y. Chen, B. J. Wang, T. Y. Hou, X. D. Hu, X. Li, X. H. Sun, S. Cai, H. M. Ji and C. M. Zheng, *Chin. Chem. Lett.*, 2018, **29**, 187-190.

13. H. J. Ye, H. Q. Li, F. Q. Jiang, J. Yin and H. Zhu, *Electrochim. Acta*, 2018, **266**, 170-177.

14. J. J. Cai, Z. S. Li and P. K. Shen, *ACS Appl. Mater. Interfaces*, 2012, **4**, 4093-4098.

15. Z. G. Wu, F. Y. Wang, S. Y. Zuo, S. K. Li, B. S. Geng, R. F. Zhuo and P. X. Yan, *J. Nanomater.*, 2015, **5**, 412515.

16. S. G. Zhang, H. Q. Zhao, M. Wang, Z. Li and J. Mi, *Electrochim. Acta*, 2018, **279**, 186-194.

17. S. P. Chen, K. Xing, J. H. Wen, M. Wen, Q. S. Wu and Y. Cui, *J. Mater. Chem. A*, 2018, **6**, 7631-7638.

18. M. Wang, Y. Zhou, J. F. Duan and D. Z. Chen, *Chin. Phys. B*, 2016, **25**, 5.

19. S. K. Li, J. X. Zheng, S. Y. Zuo, Z. G. Wu, P. X. Yan and F. Pan, *RSC Adv.*, 2015, **5**, 46941-46946.

20. S. K. Li, J. X. Zheng, Z. X. Hu, S. Y. Zuo, Z. G. Wu, P. X. Yan and F. Pan, *RSC Adv.*, 2015, **5**, 72857-72862.

21. Y. Li, J. P. Tu, X. H. Huang, H. M. Wu and Y. F. Yuan, *Electrochemistry Communications*, 2007, **9**, 49-53.

22. P. Xue, N. N. Wang, Y. X. Wang, Y. H. Zhang, Y. L. Liu, B. Tang, Z. C. Bai and S. X. Dou, *Carbon*, 2018, **134**, 222-231.

23. J. J. Ai, Y. K. Lei, S. Yang, C. Y. Lai and Q. J. Xu, *Chem. Eng. J.*, 2019, **357**,

150-158.

24. H. Jia, M. Dirican, N. Sun, C. Chen, P. Zhu, C. Y. Yan, X. Dong, Z. Du, J. S. Guo, Y. Karaduman, J. S. Wang, F. C. Tang, J. S. Tao and X. W. Zhang, *Chem. Commun.*, 2019, **55**, 505-508.

25. Y. P. Wang, Y. F. Zhang, J. R. Shi, A. Q. Pan, F. Jiang, S. Q. Liang and G. Z. Cao, *J. Mater. Chem. A*, 2018, **6**, 18286-18292.